A conservative and variation preserving finite volume method for non-overlapping meshes of reaction and diffusion in angiogenesis

Xiaoming Zheng *, Yeonhyang Kim, Leela Rakesh, En-Bing Lin

Department of Mathematics, Central Michigan University, Mount Pleasant, MI 48859, United States

HIGHLIGHTS

- Reaction and diffusion of growth factors in angiogenesis.
- Reaction and the diffusion meshes are non-overlapping.
- Conservative and reaction-variation preserving finite volume method.
- Handle non-uniform discretization and arbitrary shaped reaction domains.

## ARTICLE INFO

ABSTRACT

We propose a conservative and variation preserving finite volume method for reaction and diffusion in angiogenesis. The reaction domain keeps changing the morphology and length, and its mesh is non-uniform and does not overlap with the diffusion mesh. These facts make it very challenging to develop a numerical method that conserves the mass when transferring data between the reaction and diffusion domains. We prove the method developed in this work not only conserves the mass locally but also retains the variation in the reaction domain. In contrast, the direct interpolation may smear out the reaction data in the data transfer process. This method is applied to the growth factor reaction and diffusion problems in angiogenesis.

© 2014 Elsevier B.V. All rights reserved.

1. Introduction

Angiogenesis, the formation of new blood vessels, is crucial to many processes such as wound healing and cancer. It is controlled by growth factors such as Vascular Endothelial Growth Factor (VEGF). VEGF is released by injured tissue or hypoxic cancer cells and diffuses in the tissue. Once reaching blood vessels, VEGF binds to receptors such as VEGFR2 on endothelial cells (ECs) that line the blood vessel. The activation of VEGFR2 triggers a sequence of intracellular events resulting in cell proliferation and migration. These new blood vessels are called capillaries because they are very thin. Their diameter is at most 20 μm, but the length can extend to the size of the tissue, for example, 2 mm in diameter of a rat cornea [1] or a dormant tumor [2]. The reaction (binding kinetics) occurs only on thin capillaries, but the diffusion happens in the whole tissue domain.

---

* Corresponding author. Tel.: +1 989 734 4469.
   E-mail address: zheng1x@cmich.edu (X. Zheng).
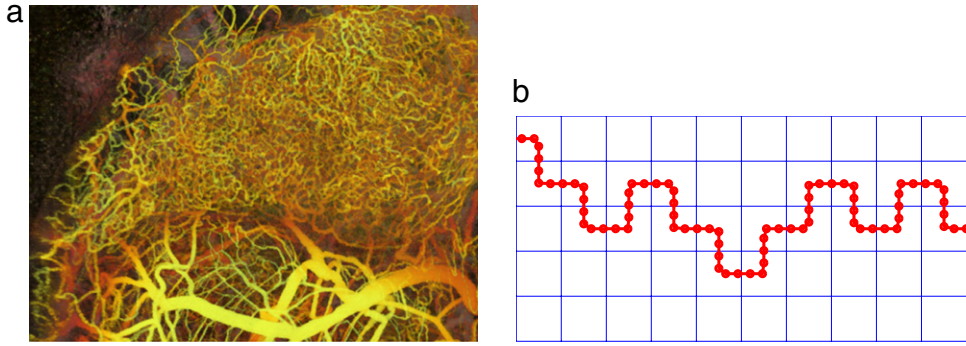
Fig. 1. (a) The highly irregular and tortuous blood vessel capillaries in a xenotransplanted U87 human glioblastoma multiforme tumor (upper part) in a mouse brain. The size of this tissue is 2.6 mm by 2 mm. This picture is taken from [12] with permissions. (b) multi-resolution of diffusion and reaction domains/meshes. The square meshlines are for the diffusion domain, and the irregular line represents a capillary centerline where the dots are the reaction mesh points.

The real problem is three-dimensional (3-D) but for simplicity we only consider a two-dimensional (2-D) tissue, denoted as Ω. Note that the proposed numerical method and its properties can be straightforwardly extended to the 3-D case. We denote the capillary domain as $\Omega_C \subset \Omega$, which is the collection of all capillaries in Ω. For simplicity, we assume the capillaries are of the uniform diameter d_c. Denote the centerline of the capillaries as Σ, its arc length parameter as s, and its spatial point as $\mathbf{x}(s)$.

Denote u as the concentration of the free growth factor, and $[FR]$ and $[BR]$ as the concentrations of free receptors and growth factor/receptor complexes (or bound receptors), respectively. The mathematical model of our study can be written as (e.g. [3,4])

$$\frac{\partial u}{\partial t} + H_{\Omega_C}\vec{v} \cdot \nabla u = D\nabla^2 u + H_{\Omega_C}f(u) \quad \text{in } \Omega, \tag{1}$$

where H_{Ω_C} is the Heaviside function of the domain Ω_C, $\vec{v}$ is the velocity of the capillary, and D is the diffusion constant. The term $H_{\Omega_C}\vec{v} \cdot \nabla u$ models the convection of growth factor by the capillary. The reaction function "f" represents the reaction on the capillary. One often used example (e.g. [4]) considers the binding kinetics between the growth factor and its receptor:

$$\begin{cases} f(u) = -k_{\text{on}}u[FR] + k_{\text{off}}[BR], \\ \dfrac{\partial [FR]}{\partial t} + H_{\Omega_C}\vec{v} \cdot \nabla [FR] = -k_{\text{on}}u[FR] + k_{\text{off}}[BR] + k_p[BR], \\ \dfrac{\partial [BR]}{\partial t} + H_{\Omega_C}\vec{v} \cdot \nabla [BR] = k_{\text{on}}u[FR] - k_{\text{off}}[BR] - k_p[BR] \end{cases} \quad \text{in } \Omega_C, \tag{2}$$

where k_{on}, k_{off}, and k_p are rates of association, disassociation, and internalization, respectively. In this model, the sum of free receptors and bound receptors is constant, denoted as $R_T \triangleq [FR] + [BR]$.

The growth factor model (1) and (2) are usually combined with a capillary growth model. There are mainly two types of capillary growth models: lattice models and non-lattice models [5]. In lattice models such as [6,5], all the mesh points of a capillary is a subset of the diffusion mesh points. That is, the reaction sites and the diffusion sites are identical. In this case, there is no need to transfer data between the reaction and diffusion meshes. However, in many non-lattice models such as [7,8,5,9,10,3,4] and this work, the capillary mesh (reaction mesh) and the diffusion mesh do not overlap. In this case, the growth factor has two expressions: one on the reaction mesh and the other on the diffusion mesh. To connect the reaction and diffusion processes, a data transfer between the two meshes is required.

We have two criteria in developing the data transfer algorithm between the non-overlapping meshes: mass conservation and reaction data variation preserving. When a quantity is expressed on two different meshes, it is natural to expect that these two expressions are identical in some measure. The measure we use is the mass conservation that includes both the local conservation (Theorem 4) and the global conservation (Theorem 5). The accurate computation of growth factors on the capillary is very important because their concentrations and variations can directly determine the fate of ECs. For example, the viability and proliferation of ECs are directly controlled by the VEGF concentrations, and the variation of VEGF along the capillary determines the direction of EC migration [11,4]. Therefore, it is critical to conserve the mass locally and preserve the variation of data in the reaction domain when designing the data transfer algorithm.

To the best of our knowledge, this work is the first to address these two criteria among numerical methods for reaction and diffusion on non-overlapping meshes. In this study, the diffusion domain is discretized with a uniform Cartesian mesh and the reaction domain is discretized with a non-lattice method. In general, the reaction mesh points are not uniform along the capillary and they are not overlapping with the diffusion mesh points or center points (see Fig. 1(b)). Furthermore, the reaction mesh points keep changing positions during capillary growth. These facts pose a big challenge in developing a data
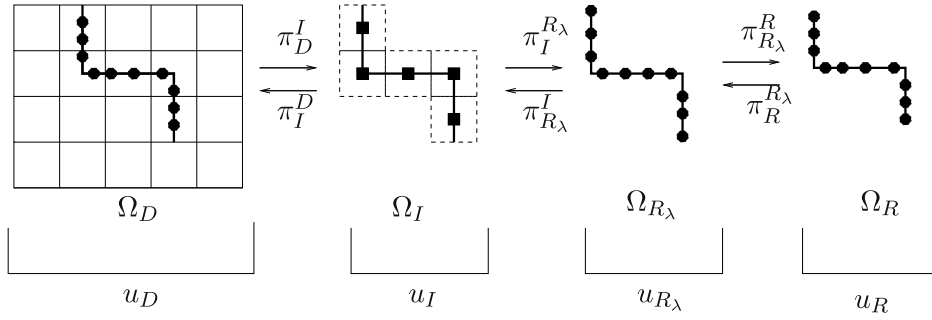
Fig. 2. Illustration of reaction and diffusion domains. Ω_D is the 2-D diffusion domain with a uniform Cartesian mesh. Ω_I is the 1-D domain aligned with Ω_D centerlines to fit the capillary. Ω_{R_λ} is the stretched capillary domain with the same length as Ω_I. Ω_R is the real capillary where reactions are solved.

transfer algorithm that satisfies the above two criteria. For instance, the direct data interpolation may produce catastrophic results, as proved in Theorem 2 and demonstrated in Section 3.1.

The rest of the paper is laid out as follows. In Section 2 we present the details of the Conservative and Variation Preserving Finite Volume Method and prove its conservation properties. In Section 3 we show some numerical simulations for VEGF reaction and diffusion in angiogenesis. We conclude in Section 4.

2. A conservative and variation preserving finite volume method

2.1. A simple capillary growth algorithm

A full capillary growth model depending on growth factors can be found in [4]. To focus on the reaction and diffusion mechanisms, we adopt a very simple capillary growth algorithm here. Denote its mesh points as $\mathbf{x}_j$, $j = 1, \ldots, m$, where $\mathbf{x}_1$ is the root and $\mathbf{x}_m$ is the tip. Denote their arc length as $s_j(t)$ at time t. The root $\mathbf{x}_1$ is fixed in space and we let $s_1(t) = 0$, for all time. The total capillary length at time t is equal to the arc length of the tip, $s_m(t)$. Assume the growth speed of the tip is a constant U and the speed of point j is $\frac{j-1}{m-1}U$. All trailing points follow the tip by migrating on the path of the tip. In other words, the capillary is the path of the tip. Therefore, the arc length of point j is $s_j(t) = s_j(0) + \frac{j-1}{m-1}Ut$ and its spatial coordinate $\mathbf{x}_j$ can be calculated with its arc length along the capillary. To mimic the tortuous shape of capillaries, we allow the capillary to make turns which is a stochastic process. The tip can turn if it extends more than the distance L_0 from the last turning point or the root. We denote the positive/negative x-direction as East/West, the positive/negative y-direction as North/South. We assume the tip mainly migrates to East, and it can only turn from South/North to East, and vice versa. If the tip points to North or South before turning, then the probability of its turning East is p_1, and the probability of its not turning is $1 - p_1$. If the tip points to East before turning, then the probability of its turning South/North is p_2, and the probability of its not turning is $1 - 2p_2$. One example of a capillary generated by this algorithm is illustrated in Fig. 1(b).

2.2. Data transfer between reaction and diffusion domains

Let $\Omega = [0, L]^2$ where L is the tissue size. In the 2-D case, the capillary cross-section becomes a line segment of length d_c. To best represent the capillary domain Ω_C in Ω, we discretize Ω with a uniform Cartesian mesh and mesh size $h = d_c$.

The tissue domain with this specific mesh is denoted as Ω_D. The capillary centerline Σ is discretized by an ordered sequence of points. For simplicity, we enforce all points to migrate along the centerlines of the Ω_D mesh, which are defined as the horizontal or vertical lines connecting center points of mesh boxes. A *mesh box* refers to a rectangle delineated by two neighboring horizontal meshlines and two neighboring vertical meshlines in Ω_D. We denote Ω_R as the domain Σ associated with the discrete points. In general, the length of Ω_R is not an integer multiple of h. In order to facilitate the data transfer between Ω_D and Ω_R, we first find a curve Ω_I along Ω_D centerlines that is the best fit of Ω_R and whose length is an integer multiple of h. Then we stretch or compress Ω_R to obtain Ω_{R_λ}, which is of the same length as Ω_I. The relationships between these domains and meshes are shown in Fig. 2.

Specifically, we define the following domains and finite volume spaces.

Ω_D, V_D: Suppose there are N mesh boxes in the diffusion domain Ω_D, denoted as B_k, $k = 1, \ldots, N$. Denote the center point of B_k as $\mathbf{x}^k = (x_1^k, x_2^k)$, then B_k is defined as $B_k = \{\mathbf{x} = (x_1, x_2) \in \Omega : |x_i - x_i^k| < h/2, \ i = 1, 2\}$. Introduce basis functions $\phi_1^D, \ldots, \phi_N^D$, each of which is the set indicator function of B_k. Define $V_D = \text{span}\{\phi_1^D, \ldots, \phi_N^D\}$. Denote the mean value of u on the box i as u_i, i.e., $u_i(t) = \frac{1}{h^2} \int_{B_i} u(\mathbf{x}, t)d\mathbf{x}$, then u has a piecewise constant representation $\sum_{i=1}^{N} u_i(t)\phi_i^D$.

Ω_R, V_R: Denote the mesh points on Ω_R as $\mathbf{x}_j^R$, $j = 1, \ldots, m$, in the order from the root to the tip of the capillary, and denote their arc lengths as s_j^R, where $s_1^R = 0$. Denote the length of the capillary as L_{Ω_R}, then $s_m^R = L_{\Omega_R}$. Denote

the interval centered around s_j^R as $[\xi_j^R, \xi_{j+1}^R]$, where $\xi_1^R = 0$, $\xi_2^R = \frac{s_1^R + s_2^R}{2}$, ..., $\xi_j^R = \frac{s_{j-1}^R + s_j^R}{2}$, $\xi_{m+1}^R = s_m^R$. Therefore, a one-dimensional notation of Ω_R with its finite volume intervals is

$$\Omega_R = [0, L_{\Omega_R}] \quad \text{with intervals } [\xi_j^R, \xi_{j+1}^R], \ j = 1, \ldots, m.$$

On Ω_R, introduce set indicator functions ψ_j^R, $j = 1, \ldots, m$, where each ψ_j^R is of value one in $[\xi_j^R, \xi_{j+1}^R]$ and zero at all other intervals. Define $V_R = \text{span} \{\psi_1^R, \ldots, \psi_m^R\}$.

Ω_I, V_I: Choose all the mesh boxes of Ω_D that contain one portion of the curve Σ whose length is more than $h/2$, and denote them as B_i^I, $i = 1, \ldots, n$, in the order from the root to the tip of the capillary. These are called *interface boxes*. For each B_i^I, the center point is denoted as $\mathbf{x}_i^I$ and the corresponding basis function as ϕ_i^I. Then connect the center points of all the interface boxes to form a one-dimensional curve, denoted as Ω_I. Assign the arc length parameter s^I to Ω_I, and denote, in each interface box B_i^I, the first point on Ω_I as $s_i^I = (i-1)h$ and the last point as $s_{i+1}^I = ih$. The length of Ω_I is $L_{\Omega_I} = nh$. The equivalent one-dimensional notation of Ω_I is

$$\Omega_I = [0, L_{\Omega_I}] \quad \text{with uniform mesh points } 0 = s_1^I < \cdots < s_{n+1}^I = L_{\Omega_I}.$$

On Ω_I, define the basis functions as ϕ_i^I, $i = 1, \ldots, n$, where ϕ_i^I is equal to 1 on the interval $[s_i^I, s_{i+1}^I]$ and zero otherwise. Define $V_I = \text{span} \{\phi_1^I, \ldots, \phi_n^I\}$.

$\Omega_{R_\lambda}, V_{R_\lambda}$: Let $\lambda = \frac{L_{\Omega_I}}{L_{\Omega_R}}$, which typically is not equal to 1. To facilitate the data transfer between Ω_D and Ω_R, we further introduce a new domain $\Omega_{R_\lambda} = \lambda \Omega_R$, i.e.,

$$\Omega_{R_\lambda} = [0, L_{\Omega_I}] \quad \text{with intervals } [\xi_j^{R_\lambda}, \xi_{j+1}^{R_\lambda}], \ \xi_j^{R_\lambda} = \lambda \xi_j^R, \ j = 1, \ldots, m.$$

The basis functions in V_R are stretched to obtain basis functions $\psi_j^{R_\lambda}$, $j = 1, \ldots, m$ on Ω_{R_λ} by letting $\psi_j^{R_\lambda}(\xi) = \psi_j^R(\xi/\lambda)$, where $\xi \in \Omega_{R_\lambda}$. Define $V_{R_\lambda} = \text{span} \{\psi_1^{R_\lambda}, \ldots, \psi_m^{R_\lambda}\}$.

Therefore, V_R, V_{R_λ}, and V_I are all piecewise constant function spaces, and their lengths satisfy $L_{\Omega_I} = L_{\Omega_{R_\lambda}} = \lambda L_{\Omega_R} = nh$.

We define two projections $\pi_{R_\lambda}^I$ and $\pi_I^{R_\lambda}$, two stretching/compression operators $\pi_R^{R_\lambda}$ and $\pi_{R_\lambda}^R$, and two restriction/expansion operators π_D^I and π_I^D as follows.

(1) $\pi_{R_\lambda}^I : V_{R_\lambda} \to V_I$, for any $u \in V_{R_\lambda}$,

$$\left(\pi_{R_\lambda}^I(u), v\right)_{L_2} = (u, v)_{L_2}, \quad \forall v \in V_I; \tag{3}$$

(2) $\pi_I^{R_\lambda} : V_I \to V_{R_\lambda}$, for any $u \in V_I$,

$$\left(\pi_I^{R_\lambda}(u), v\right)_{L_2} = (u, v)_{L_2}, \quad \forall v \in V_{R_\lambda}; \tag{4}$$

(3) $\pi_R^{R_\lambda} : V_R \to V_{R_\lambda}$, for any $u_R \in V_R$,

$$\pi_R^{R_\lambda}(u_R)(s) = \frac{1}{\lambda} u_R\left(\frac{s}{\lambda}\right), \quad \forall s \in [0, L_{\Omega_{R_\lambda}}]; \tag{5}$$

(4) $\pi_{R_\lambda}^R : V_{R_\lambda} \to V_R$, for any $u_{R_\lambda} \in V_{R_\lambda}$,

$$\pi_{R_\lambda}^R(u_{R_\lambda})(s) = \lambda u_{R_\lambda}(\lambda s), \quad \forall s \in [0, L_{\Omega_R}]; \tag{6}$$

(5) $\pi_D^I : V_D \to V_I$, for any $u_D = \sum_{i=1}^N u_{D_i} \phi_i^D \in V_D$, assuming $\phi_{i_j}^D|_{\Omega_I} = \phi_j^I$, $j = 1, \ldots, n$,

$$\pi_D^I(u_D) = \sum_{j=1}^n u_{D_{i_j}} \phi_j^I; \tag{7}$$

(6) $\pi_I^D : V_I \to V_D$, for any $u_I = \sum_{j=1}^n u_{I_j} \phi_j^I \in V_I$, assuming $\phi_{i_j}^D|_{\Omega_I} = \phi_j^I$, $j = 1, \ldots, n$,

$$\pi_I^D(u_I) = \sum_{j=1}^n u_{I_j} \phi_{i_j}^D. \tag{8}$$

The inner product $(u, v)_{L_2}$ in Eqs. (3) and (4) is defined by $\int u(s)v(s)ds$. The relationship between these operators and spaces is illustrated in Fig. 2. It is easy to see from (3) and (4) that both $\pi_I^{R_\lambda}$ and $\pi_{R_\lambda}^I$ reserve the mass, that is, $\int_{\Omega_{R_\lambda}} \pi_I^{R_\lambda}(u^I)d\xi^{R_\lambda} = \int_{\Omega_I} u^I ds$, $\forall u^I \in V_I$, and $\int_{\Omega_I} \pi_{R_\lambda}^I(u^{R_\lambda})ds = \int_{\Omega_{R_\lambda}} u^{R_\lambda} d\xi^{R_\lambda}$, $\forall u^{R_\lambda} \in V_{R_\lambda}$. Further, we define two combined operators $\pi_R^I = \pi_{R_\lambda}^I \circ \pi_R^{R_\lambda}$ and $\pi_I^R = \pi_{R_\lambda}^R \circ \pi_I^{R_\lambda}$. It can be easily verified that

Lemma 1. *For any $u_R \in V_R$ and $u_I \in V_I$,*

$$\left(\pi_R^I(u_R), v_I\right)_{L_2(\Omega_I)} = (u_R, v_I(\lambda\cdot))_{L_2(\Omega_R)}, \quad \forall v_I \in V_I;$$

$$\left(\pi_I^R(u_I), v_R\right)_{L_2(\Omega_R)} = \left(u_I, v_R\left(\frac{\cdot}{\lambda}\right)\right)_{L_2(\Omega_I)}, \quad \forall v_R \in V_R.$$

Lemma 2.

$$\int_{\Omega_D} \pi_I^D(u_I)ds = h \int_{\Omega_I} u_I ds, \quad \forall u_I \in V_I.$$

Proof. Notice that both Ω_D and Ω_I are of uniform mesh size h. So $\int_{\Omega_I} \phi_j^I ds = h$, $j = 1, \ldots, n$, and $\int_{\Omega_D} \phi_i^D d\mathbf{x} = h^2$, $i = 1, \ldots, N$. Therefore, for any $u_I = \sum_{j=1}^n u_{I_j} \phi_j^I$,

$$\int_{\Omega_D} \pi_I^D(u_I)d\mathbf{x} \overset{\text{Eq. (8)}}{=} \sum_{j=1}^n \int_{\Omega_I} u_{I_j} \phi_{i_j}^D(\mathbf{x})d\mathbf{x} = \sum_{j=1}^n u_{I_j} h^2 = h \sum_{j=1}^n \int_{\Omega_I} u_{I_j} \phi_j^I(s)ds = h \int_{\Omega_I} u_I ds. \quad \square$$

Remark 1. In the 3-D case, Lemma 2 becomes $\int_{\Omega_D} \pi_I^D(u_I)ds = h^2 \int_{\Omega_I} u_I ds$.

2.3. Relations between π_R^I and π_I^R

The operators π_R^I and π_I^R are crucial to the data transfer between the reaction and diffusion domains. A key observation of their relationship is that $\pi_R^{R_\lambda}$ is an isomorphism from V_R to V_{R_λ} and $\pi_{R_\lambda}^R$ is the inverse. Therefore, we only need to study the interactions between $\pi_{R_\lambda}^I$ and $\pi_I^{R_\lambda}$.

As an immediate consequence of Eqs. (3) and (4), we have the following lemma.

Lemma 3. *For any $u \in V_{R_\lambda}$, $v \in V_I$,*

$$\pi_{R_\lambda}^I(u) = \sum_{i=1}^n M_i^I(u)\phi_i^I, \qquad \pi_I^{R_\lambda}(v) = \sum_{j=1}^m M_j^{R_\lambda}(v)\psi_j^{R_\lambda}, \tag{9}$$

where $M_i^I(u)$ is the mean value of u in (s_i, s_{i+1}) and $M_j^{R_\lambda}(v)$ is the mean value of v in $(\xi_j^{R_\lambda}, \xi_{j+1}^{R_\lambda})$.

We denote the sets of mesh points of Ω_I, Ω_{R_λ}, and Ω_R as S_I, S_{R_λ}, and S_R, respectively. That is, $S_I = \{s_1^I, s_2^I, \ldots, s_n^I, s_{n+1}^I\}$, $S_{R_\lambda} = \{\xi_1^{R_\lambda}, \xi_2^{R_\lambda}, \ldots, \xi_m^{R_\lambda}, \xi_{m+1}^{R_\lambda}\}$, and $S_R = \{\xi_1^R, \xi_2^R, \ldots, \xi_m^R, \xi_{m+1}^R\}$. We denote the sets of interior mesh points of Ω_I, Ω_{R_λ}, and Ω_R as $\mathring{S}_I$, $\mathring{S}_{R_\lambda}$, and $\mathring{S}_R$, respectively. That is, $\mathring{S}_I = \{s_2^I, \ldots, s_n^I\}$, $\mathring{S}_{R_\lambda} = \{\xi_2^{R_\lambda}, \ldots, \xi_m^{R_\lambda}\}$, and $\mathring{S}_R = \{\xi_2^R, \ldots, \xi_m^R\}$.

Theorem 1. (i) $\pi_I^{R_\lambda} \circ \pi_{R_\lambda}^I = \text{Id}_{V_{R_\lambda}}$ *if and only if* $S_{R_\lambda} \subseteq S_I$.
(ii) $\pi_{R_\lambda}^I \circ \pi_I^{R_\lambda} = \text{Id}_{V_I}$ *if and only if* $S_I \subseteq S_{R_\lambda}$.

Proof. We only need to prove (i) because (ii) is similar.

(i) "$\Rightarrow$": We will prove by contradiction. Assume there is some point $\xi_{j_0}^{R_\lambda} \in S_{R_\lambda}$, but $\xi_{j_0}^{R_\lambda} \notin S_I$. Suppose $\xi_{j_0}^{R_\lambda} \in (s_k^I, s_{k+1}^I)$. Then $M_k^I(\psi_{j_0}^{R_\lambda}) > 0$ and $M_{j_0-1}^{R_\lambda}(\phi_k^I) > 0$. Furthermore, $M_i^I(\psi_{j_0}^{R_\lambda}) \geq 0$ and $M_{j_0-1}^{R_\lambda}(\phi_i^I) \geq 0$ for each $i = 1, \ldots, n$. Let $\xi_0 = (\max\{s_k^I, \xi_{j_0-1}^{R_\lambda}\} + \xi_{j_0}^{R_\lambda})/2$, then $s_k^I < \xi_0 < \xi_{j_0}^{R_\lambda}$. On one hand $\psi_{j_0}^{R_\lambda}(\xi_0) = 0$ because the support of $\psi_{j_0}^{R_\lambda}$ is $[\xi_{j_0}^{R_\lambda}, \xi_{j_0+1}^{R_\lambda}]$. On the other hand we have

$$\pi_I^{R_\lambda} \circ \pi_{R_\lambda}^I(\psi_{j_0}^{R_\lambda})(\xi_0) = \pi_I^{R_\lambda} \circ \left(\sum_{i=1}^n M_i^I(\psi_{j_0}^{R_\lambda})\phi_i^I\right)(\xi_0)$$

$$= \sum_{i=1}^n M_i^I(\psi_{j_0}^{R_\lambda}) \sum_{j=1}^m M_j^{R_\lambda}(\phi_i^I)\psi_j^{R_\lambda}(\xi_0)$$

$$= \sum_{i=1}^n M_i^I(\psi_{j_0}^{R_\lambda})M_{j_0-1}^{R_\lambda}(\phi_i^I)$$

$$\geq M_k^I(\psi_{j_0}^{R_\lambda})M_{j_0-1}^{R_\lambda}(\phi_k^I) > 0.$$

This is a contradiction to $\pi_I^{R_\lambda} \circ \pi_{R_\lambda}^I = \text{Id}_{V_{R_\lambda}}$.

(i) "⇐": if $S_{R_\lambda} \subseteq S_I$, then for each interval $[\xi_j^{R_\lambda}, \xi_{j+1}^{R_\lambda}]$ of Ω_{R_λ}, there exist $s_{k_1}^I, s_{k_2}^I \in S_I$ such that $[\xi_j^{R_\lambda}, \xi_{j+1}^{R_\lambda}] = [s_{k_1}^I, s_{k_2}^I]$. According to Lemma 3, we have $\pi_{R_\lambda}^I(\psi_j^{R_\lambda}) = \chi_{[s_{k_1}^I, s_{k_2}^I]}$, where $\chi_{[s_{k_1}^I, s_{k_2}^I]}$ is of value one in the interval $[s_{k_1}^I, s_{k_2}^I]$ and zero otherwise. Using Lemma 3 again, we obtain $\pi_I^{R_\lambda} \circ \pi_{R_\lambda}^I(\psi_j^{R_\lambda}) = \psi_j^{R_\lambda}$. Because j is arbitrary, $\pi_I^{R_\lambda} \circ \pi_{R_\lambda}^I = \mathrm{Id}_{V_{R_\lambda}}$. □

Corollary 1. (i) $\pi_I^R \circ \pi_R^I = \mathrm{Id}_{V_R}$ if and only if $\lambda S_R \subseteq S_I$.
(ii) $\pi_R^I \circ \pi_I^R = \mathrm{Id}_{V_I}$ if and only if $S_I \subseteq \lambda S_R$.

The conditions $\lambda S_R \subseteq S_I$ and $S_I \subseteq \lambda S_R$ are almost impossible to hold because the capillary points change positions arbitrarily in every time step of our capillary growth algorithm. Thus, in general, after one operation of $\pi_I^R \circ \pi_R^I$ some information of the data will be lost. In numerical simulations, such an operation may be performed in every time step. The following theorem shows that after sufficiently many steps, the data will converge to its mean value.

Theorem 2. If $\mathring{S}_{R_\lambda} \cap \mathring{S}_I = \emptyset$, then for any $u \in V_{R_\lambda}$,

$$\lim_{k \to \infty} (\pi_I^{R_\lambda} \circ \pi_{R_\lambda}^I)^k(u) = \frac{1}{L_{\Omega_{R_\lambda}}} \int_{\Omega_{R_\lambda}} u(\xi^{R_\lambda}) d\xi^{R_\lambda}.$$

Proof. First, we note that by Lemma 3 for any $v \in V_I$, $\max(\pi_I^{R_\lambda}(v)) \le \max(u)$ and $\min(\pi_{R_\lambda}^I(v)) \ge \min(v)$. Similarly for any $u \in V_{R_\lambda}$, we have $\max(\pi_{R_\lambda}^I(u)) \le \max(u)$ and $\min(\pi_{R_\lambda}^I(u)) \ge \min(u)$. Denote $P = \pi_I^{R_\lambda} \circ \pi_{R_\lambda}^I$. Therefore, $\max P(u) \le \max(u)$ and $\min P(u) \ge \min(u)$, which implies $\|P^{k+1}(u)\|_{L^\infty} \le \|P^k(u)\|_{L^\infty} \le \|u\|_{L^\infty}$, $\forall k \in \mathbb{N}$. So $\{P^k(u), k \in \mathbb{N}\}$ is a bounded subset in the finite dimensional space V_{R_λ} with the L^∞ norm. Then it must have a convergent subsequence, which is denoted as $\{P^{k_i}(u), i \in \mathbb{N}\}$ and its limit is denoted as $u_0 \in V_{R_\lambda}$. By the dominant convergence theorem, $\int_{\Omega_{R_\lambda}} u_0 = \int_{\Omega_{R_\lambda}} u$. Since $\max(P^k(u)) \le \max(u)$ and $\min(P^k(u)) \ge \min(u)$, $\forall k \in \mathbb{N}$, we have $\max(u_0) \le \max(u)$ and $\min(u_0) \ge \min(u)$.

Second, we shall prove that $\max u_0 = \min u_0$, that is, u_0 is a constant. Assume the contrary is true, that is, $\max(u_0) > \min(u_0)$. Without loss of generality, we assume (ξ_j, ξ_{j+1}) is the last interval taking the maximum value and $j < m$. Suppose $\xi_{j+1} \in (s_i, s_{i+1}) \subset \Omega_I$. By Lemma 3, $\pi_{R_\lambda}^I(u_0)|_{(s_i,s_{i+1})}$ is the mean value of u_0 in (s_i, s_{i+1}). Because u_0 is strictly less than $\max(u_0)$ in the non-empty interval $(\xi_{j+1}, \xi_{j+2}) \cap (s_i, s_{i+1})$, $\pi_{R_\lambda}^I(u_0)|_{(s_i,s_{i+1})}$ is also strictly less than $\max(u_0)$. On the other hand, when mapped back to V_{R_λ}, $\pi_{R_\lambda}^I(u_0)|_{(s_i,s_{i+1})}$ has a non-zero contribution to the value $\pi_I^{R_\lambda} \circ \pi_{R_\lambda}^I(u_0)_{(\xi_j,\xi_{j+1})}$ through the non-empty interval $(\xi_j, \xi_{j+1}) \cap (s_i, s_{i+1})$. Therefore, $\pi_I^{R_\lambda} \circ \pi_{R_\lambda}^I(u_0)|_{(\xi_j,\xi_{j+1})}$ is also strictly less than $\max(u_0)$. Ω_{R_λ} has m intervals, so u_0 has at most $m-1$ maximum intervals. Then after m steps P-iterations, $\max(P^m(u_0)) < \max(u_0)$. Let $\delta = \max(u_0) - \max(P^m(u_0))$. It is easy to tell that $P^m(u_0)$ is the limit of another subsequence $\{P^{k_i+m}(u), i \in \mathbb{N}\}$. Then there exists $K \in \mathbb{N}$ so that $\forall k_i > K$, $\|P^{k_i+m}(u) - P^m(u_0)\|_\infty \le \delta/2$. So $|\max(P^m(u_0)) - \max(P^{k_i+m}(u))| \le \|P^{k_i+m}(u) - P^m(u_0)\|_\infty \le \delta/2$. Since $\max(P^{k_i+m}(u))$ is a decreasing function of k_i, $0 \le \max(P^{k_i+m}(u)) - \max(P^m(u_0)) \le \delta/2$. Furthermore, $\forall k_j > k_i + m$, $\max(P^{k_j}(u)) \le \max((P^{k_i+m}(u))) \le \max((P^m(u_0))) + \delta/2 = \max(u_0) - \delta/2$. Therefore, $\|P^{k_j}(u) - u_0\|_\infty \ge \max(u_0) - \max(P^{k_j}(u)) \ge \delta/2$. This is contradictory to the assumption that u_0 is the limit of $\{P^{k_j}(u), k_j \in \mathbb{N}\}$. Therefore, u_0 must be a constant.

Finally, since $\max(P^k(u)) - \min(P^k(u))$ is a decreasing function of k, and one subsequence is of limit zero, therefore, as for the whole sequence, $\lim_{k \to \infty}(\max(P^k(u)) - \min(P^k(u))) = 0$. Thus, the whole sequence converges to a constant. □

Corollary 2. If $(\lambda \mathring{S}_R) \cap \mathring{S}_I = \emptyset$, then $\lim_{k \to \infty}(\pi_I^R \circ \pi_R^I)^k(u) = \frac{1}{L_{\Omega_R}} \int_{\Omega_R} u(\xi^R) d\xi^R$, $\forall u \in V_R$.

2.4. A conservative and variation preserving finite volume method

Because the capillaries keep changing its morphology in time, we denote the capillary domain at time step t^k as $\Omega_{R(k)}$. The same rule is applied to associated domains and operators, such as $\Omega_{I(k)}$, $\pi_{R_\lambda(k)}^{I(k)}$, $\pi_{R(k)}^{R_\lambda(k)}$, etc. Assume at the time step $t^{k-1} = (k-1)\Delta t$, $k = 1, 2, \ldots$, we have obtained the capillary domain $\Omega_{R(k-1)} = \cup_{i=1}^m [\xi_i^{R(k-1)}, \xi_{i+1}^{R(k-1)}]$, the solution u_D^{k-1} in V_D, and the solution $u_{R(k-1)}^{k-1}$, $[FR]_{R(k-1)}^{k-1}$, and $[BR]_{R(k-1)}^{k-1}$ in $V_{R(k-1)}$. Note that the number of basis functions of $V_{R(k)}$ is a fixed number denoted by m but the number of basis of $V_{I(k)}$ depends on time, i.e., $n = n(k)$. Now we proceed to time step t^k to compute the solutions u_D^k, $u_{R(k)}^k$, $[FR]_{R(k)}^k$, and $[BR]_{R(k)}^k$.

2.4.1. Capillary growth step

Using the capillary growth algorithm described in Section 2.1, we compute the new capillary domain $\Omega_{R(k)} = \cup_{i=1}^m [\xi_i^{R(k)}, \xi_{i+1}^{R(k)}]$. Then determine domains $\Omega_{I(k)}$ and $\Omega_{R_\lambda(k)}$ according to the description in Section 2.2, and generate spaces $V_{I(k)} = \mathrm{span}\{\phi_1^{I(k)}, \ldots, \phi_{n(k)}^{I(k)}\}$, $V_{R(k)} = \mathrm{span}\{\psi_1^{R(k)}, \ldots, \psi_m^{R(k)}\}$, and $V_{R_\lambda(k)} = \mathrm{span}\{\psi_1^{R_\lambda(k)}, \ldots, \psi_m^{R_\lambda(k)}\}$.

We assume the capillary moves in such a manner that either $\Omega_{I(k-1)} \subset \Omega_{I(k)}$ or $\Omega_{I(k-1)} \supseteq \Omega_{I(k)}$. The former represents the capillary invading a new region, and the latter represents the capillary shrinking or remaining the same.

2.4.2. Convection step

The convection part is

$$\frac{\partial u}{\partial t} + \vec{v} \cdot \nabla u = 0 \quad \text{in } \Omega_C.$$

In the capillary growth algorithm, all points move with the capillary velocity $\vec{v}$. Then the above equation becomes $\frac{du}{dt} = 0$, where $\frac{d}{dt}$ is the material derivative. Therefore, the mean value of u on each interval $[\xi_j^R, \xi_{j+1}^R]$ is conserved in this convection step. Thus, the mean value of u becomes

$$u_{R(k),i}^{k,*} = \frac{\xi_{i+1}^{R(k-1)} - \xi_i^{R(k-1)}}{\xi_{i+1}^{R(k)} - \xi_i^{R(k)}} u_{R(k-1),i}^{k-1} \tag{10}$$

on each interval $\left[\xi_i^{R(k)}, \xi_{i+1}^{R(k)}\right]$, $i = 1, \ldots, m$. Similarly, we have $[FR]_{R(k),i}^{k,1} = \frac{\xi_{i+1}^{R(k-1)} - \xi_i^{R(k-1)}}{\xi_{i+1}^{R(k)} - \xi_i^{R(k)}}[FR]_{R(k-1),i}^{k-1}$, and $[BR]_{R(k),i}^{k,1} = \frac{\xi_{i+1}^{R(k-1)} - \xi_i^{R(k-1)}}{\xi_{i+1}^{R(k)} - \xi_i^{R(k)}}[BR]_{R(k-1),i}^{k-1}$.

Then we update u in Ω_D:

$$u_D^{k,1} = u_D^{k-1} - \pi_{I(k-1)}^D \circ \pi_D^{I(k-1)}(u_D^{k-1}) + \pi_{I(k)}^D \circ \pi_{R(k)}^{I(k)}(u_{R(k)}^{k,*}). \tag{11}$$

Note when $\Omega_{I(k-1)} \subset \Omega_{I(k)}$, the capillaries invade the region $\Omega_{I(k)} \setminus \Omega_{I(k-1)}$ and add more growth factor to the original concentration $\pi_D^{I(k)}(u_D^{k-1}) - \pi_D^{I(k-1)}(u_D^{k-1})$ there. Accordingly, we need to add the original amount to $\Omega_{R(k)}$:

$$u_{R(k)}^{k,1} = \begin{cases} u_{R(k)}^{k,*} + \pi_{I(k)}^{R(k)}\left(\pi_D^{I(k)}(u_D^{k-1}) - \pi_D^{I(k-1)}(u_D^{k-1})\right), & \text{if } \Omega_{I(k-1)} \subset \Omega_{I(k)}; \\ u_{R(k)}^{k,*}, & \text{if } \Omega_{I(k-1)} \supseteq \Omega_{I(k)}. \end{cases} \tag{12}$$

2.4.3. Reaction step

On each interval $\left[\xi_i^{R(k)}, \xi_{i+1}^{R(k)}\right]$, $i = 1, \ldots, m$, we solve the reaction equation $\frac{\partial u_{R,i}}{\partial t} = f(u_{R,i})$ and equations in (2) from t^{k-1} to t^k with the initial value $u_{R(k)}^{k,1}$, $[FR]_{R(k)}^{k,1}$ and $[BR]_{R(k)}^{k,1}$. Denote the result as $u_{R(k)}^{k,2}$, $[FR]_{R(k)}^k$, and $[BR]_{R(k)}^k$.

Afterwards, u in Ω_D is updated to

$$u_D^{k,2} = (\text{Id}_{V_D} - \pi_{I(k)}^D \circ \pi_D^{I(k)})(u_D^{k,1}) + \pi_{I(k)}^D \circ \pi_{R(k)}^{I(k)}(u_{R(k)}^{k,2}). \tag{13}$$

The time derivative of the reaction equations is approximated by the implicit trapezoidal method and the resulting nonlinear equations are solved by the Broyden method (cf. [13]).

2.4.4. Diffusion step

We solve the diffusion equation $\frac{\partial u_D}{\partial t} = D\nabla^2 u_D$ in Ω_D from t^{k-1} to t^k with input $u_D^{k,2}$ and output $u_D^{k,3}$. Then we update u on Ω_R by transferring the difference of u_D from Ω_D to Ω_R:

$$u_{R(k)}^{k,3} = u_{R(k)}^{k,2} + \pi_{I(k)}^{R(k)} \circ \pi_D^{I(k)}(u_D^{k,3} - u_D^{k,2}). \tag{14}$$

We use the standard five-point stencil to discretize the Laplace operator and the Crank–Nicolson scheme to discretize the time derivative. For details readers are referred to [14, Chapter 3]. Finally, we obtain the end-of-step data $u_D^k = u_D^{k,3}$ and $u_{R(k)}^k = u_{R(k)}^{k,3}$.

Remark 2. When this numerical method is extended to the 3-D case, the differences are only on the construction of the domain Ω_D and the operators π_D^I and π_I^D and the solution process of the diffusion equation $\frac{\partial u_D}{\partial t} = D\nabla^2 u_D$, which are all straightforward.

2.5. Reaction variation preserving

Eq. (14) is the crucial step to keep the variation of data in the reaction domain.

Theorem 3 (*Reaction Variation Preserving*). *Suppose the capillary is fixed in space and the diffusion constant D is zero. If the whole numerical method (2.4.1–2.4.4) is applied, then the value of u on the reaction domain is only determined by the numerical method of $\frac{\partial u}{\partial t} = f(u)$ and (2).*

Proof. If the capillary is fixed in space, then $\Omega_{R(k)}$, $\Omega_{I(k)}$, $V_{R(k)}$, $V_{I(k)}$ are fixed. In the convection step, we have $u_{R(k)}^{k,*} = u_{R(k-1)}^{k-1}$ from Eq. (10) and $u_{R(k)}^{k,1} = u_{R(k)}^{k,*} = u_{R(k-1)}^{k-1}$ from Eq. (12). Because $D = 0$, the diffusion step must give $u_D^{k,3} = u_D^{k,2}$ and thus $u_{R(k)}^{k,3} = u_{R(k)}^{k,2}$ according to Eq. (14). Therefore, the value of u on $\Omega_{R(k)}$ is only determined by $\frac{\partial u}{\partial t} = f(u)$ and equations in (2) in the reaction step. $\quad\square$

The strategy of (14) is the same as the wavelet method, where the average message is stored in the coarser level and the oscillation (local value minus the average value) is kept in the finer level. This can be clearly seen by rewriting (14) as

$$u_{R(k)}^{k,3} = \pi_{I(k)}^{R(k)} \circ \pi_D^{I(k)}(u_D^{k,3}) + \left[u_{R(k)}^{k,2} - \pi_{I(k)}^{R(k)} \circ \pi_D^{I(k)}(u_D^{k,2}) \right]. \tag{15}$$

On the right side of (15), the first term stands for the new average information on the coarser mesh Ω_I, and the difference in brackets represents the old oscillation on the finer mesh Ω_R.

In contrast, the direct interpolation

$$u_{R(k)}^{k,3} = \pi_{I(k)}^{R(k)} \circ \pi_D^{I(k)}(u_D^{k,3}) \tag{16}$$

would smear out the oscillation of u_R along the capillary, as proved in Theorem 2. Note that the computational costs of the direct interpolation formula (16) and the proposed formula (14) are almost identical, because the main cost of both formulas is on the same operator $\pi_{I(k)}^{R(k)} \circ \pi_D^{I(k)}$. The differences between these two formulas in numerical simulations will be demonstrated in Section 3.

2.6. Mass conservation properties

Lemma 4. If $\Omega_{I(k-1)} \subset \Omega_{I(k)}$, then $\pi_D^{I(k)} \circ \pi_{I(k-1)}^D(v) = v$, $\forall v \in V_{I(k-1)}$. If $\Omega_{I(k-1)} \supseteq \Omega_{I(k)}$, then $\pi_D^{I(k)} \circ \pi_{I(k-1)}^D \circ \pi_D^{I(k-1)}(u_D) = \pi_D^{I(k)}(u_D)$, $\forall u_D \in V_D$.

Proof. If $\Omega_{I(k-1)} \subset \Omega_{I(k)}$, then $V_{I(k-1)} \subset V_{I(k)}$ if any function in $V_{I(k-1)}$ is given a zero extension to the region $\Omega_{I(k)} \backslash \Omega_{I(k-1)}$. Let $n = \dim(V_{I(k-1)})$ and $V_{I(k-1)} = \operatorname{span}\{\phi_1^I, \ldots, \phi_n^I\}$. For each $j = 1, \ldots, n$, there exists i_j such that $\pi_{I(k-1)}^D \phi_j^I = \phi_{i_j}^D$, which implies that $\pi_D^{I(k)}(\phi_{i_j}^D) = \pi_D^{I(k-1)}(\phi_{i_j}^D) = \phi_j^I$. For any $v \in V_{I(k-1)}$, assume $v = \sum_{j=1}^n v_j \phi_j^I$. Thus, $\pi_D^{I(k)} \circ \pi_{I(k-1)}^D(v) = \pi_D^{I(k)} \circ \pi_{I(k-1)}^D(\sum_{j=1}^n v_j \phi_j^I) = \pi_D^{I(k)}(\sum_{j=1}^n v_j \phi_{i_j}^D) = \sum_{j=1}^n v_j \phi_j^I = v$.

If $\Omega_{I(k-1)} \supseteq \Omega_{I(k)}$, then $V_{I(k-1)} \supseteq V_{I(k)}$ if any function in $V_{I(k)}$ is given a zero extension to the region $\Omega_{I(k-1)} \backslash \Omega_{I(k)}$. We define $V_{I(k-1)}$ and its basis functions in the same way as in the last paragraph, and further define $V_{I(k)} = \operatorname{span}\{\phi_1^I, \ldots, \phi_m^I\}$ where $m \leq n$. For any $u_D \in V_D$, assume $u_D = \sum_{i=1}^{\dim(V_D)} u_{D_i} \phi_i^D$, then $\pi_D^{I(k-1)}(u_D) = \sum_{j=1}^n u_{D_{i_j}} \phi_j^I$. Further, for each $j = 1, \ldots, n$, there exists i_j such that $\pi_D^{I(k)}(\phi_{i_j}^D) = \phi_j^I$. Thus $\pi_D^{I(k)} \circ \pi_{I(k-1)}^D \circ \pi_D^{I(k-1)}(u_D) = \pi_D^{I(k)} \circ \pi_{I(k-1)}^D(\sum_{j=1}^n u_{D_{i_j}} \phi_j^I) = \pi_D^{I(k)}(\sum_{j=1}^n u_{D_{i_j}} \phi_{i_j}^D) = \sum_{j=1}^m u_{D_{i_j}} \phi_j^I = \pi_D^{I(k)}(u_D)$. $\quad\square$

The following theorem gives the direct comparisons between $u_D^{k,j}$ and $u_{R(k)}^{k,j}$, $j = 1, 2, 3$, on the interface domain $\Omega_{I(k)}$.

Theorem 4 (*Local Conservation*).

(i) If $\Omega_{I(k-1)} \supseteq \Omega_{I(k)}$, then $\pi_D^{I(k)}(u_D^{k,1}) = \pi_{R(k)}^{I(k)}(u_{R(k)}^{k,1})$. If $\Omega_{I(k-1)} \subset \Omega_{I(k)}$, then $\pi_D^{I(k)}(u_D^{k,1}) = \pi_{R(k)}^{I(k)}(u_{R(k)}^{k,1}) + \left(\operatorname{Id}_{V_{I(k)}} - \pi_{R(k)}^{I(k)} \circ \pi_{I(k)}^{R(k)} \right) \left(\pi_D^{I(k)}(u_D^{k-1}) - \pi_D^{I(k-1)}(u_D^{k-1}) \right)$.

(ii) $\pi_D^{I(k)}(u_D^{k,2}) = \pi_{R(k)}^{I(k)}(u_{R(k)}^{k,2})$.

(iii) $\pi_{R(k)}^{I(k)}(u_{R(k)}^{k,3}) = \pi_{R(k)}^{I(k)} \circ \pi_{I(k)}^{R(k)} \left(\pi_D^{I(k)}(u_D^{k,3}) \right) + \pi_{R(k)}^{I(k)} \left(\operatorname{Id}_{V_{R(k)}} - \pi_{I(k)}^{R(k)} \circ \pi_{R(k)}^{I(k)} \right) u_{R(k)}^{k,2}$.

Remark 3. Because of Corollary 1, we cannot expect $\pi_{R(k)}^{I(k)} \circ \pi_{I(k)}^{R(k)} = \operatorname{Id}_{V_{I(k)}}$ or $\pi_{I(k)}^{R(k)} \circ \pi_{R(k)}^{I(k)} = \operatorname{Id}_{V_{R(k)}}$ for the general capillary growth. Therefore, $\pi_D^{I(k)}(u_D^{k,1}) \neq \pi_{R(k)}^{I(k)}(u_{R(k)}^{k,1})$ when $\Omega_{I(k-1)} \subset \Omega_{I(k)}$ and $\pi_D^{I(k)}(u_D^{k,3}) \neq \pi_{R(k)}^{I(k)}(u_{R(k)}^{k,3})$.

Proof. (Part i) When $\Omega_{I(k-1)} \supseteq \Omega_{I(k)}$, apply $\pi_D^{I(k)}$ on both sides of (11), then

$$\begin{aligned}
\pi_D^{I(k)}(u_D^{k,1}) &= \pi_D^{I(k)}(u_D^{k-1}) - \pi_D^{I(k)} \circ \pi_{I(k-1)}^D \circ \pi_D^{I(k-1)}(u_D^{k-1}) + \pi_D^{I(k)} \circ \pi_{I(k)}^D \circ \pi_{R(k)}^{I(k)}(u_{R(k)}^{k,*}) \\
&= \pi_D^{I(k)}(u_D^{k-1}) - \pi_D^{I(k)}(u_D^{k-1}) + \pi_{R(k)}^{I(k)}(u_{R(k)}^{k,*}) \\
&= \pi_{R(k)}^{I(k)}(u_{R(k)}^{k,1}),
\end{aligned} \tag{17}$$

where we have used the facts that $\pi_D^{I(k)} \circ \pi_{I(k-1)}^D \circ \pi_D^{I(k-1)}(u_D^{k-1}) = \pi_D^{I(k)}(u_D^{k-1})$ by Lemma 4 and $u_{R(k)}^{k,1} = u_{R(k)}^{k,*}$ in the case of $\Omega_{I(k-1)} \supseteq \Omega_{I(k)}$.

When $\Omega_{I(k-1)} \subset \Omega_{I(k)}$, apply $\pi_D^{I(k)}$ on both sides of (11), then

$$
\begin{aligned}
\pi_D^{I(k)}(u_D^{k,1}) &= \pi_D^{I(k)}(u_D^{k-1}) - \pi_D^{I(k)} \circ \pi_{I(k-1)}^D \circ \pi_D^{I(k-1)}(u_D^{k-1}) + \pi_D^{I(k)} \circ \pi_{I(k)}^D \circ \pi_{R(k)}^{I(k)}(u_{R(k)}^{k,*}) \\
&= \pi_D^{I(k)}(u_D^{k-1}) - \pi_D^{I(k-1)}(u_D^{k-1}) + \pi_{R(k)}^{I(k)}(u_{R(k)}^{k,*}),
\end{aligned}
\tag{18}
$$

where we have used the facts that $\pi_D^{I(k)} \circ \pi_{I(k-1)}^D \circ \pi_D^{I(k-1)}(u_D^{k-1}) = \pi_D^{I(k-1)}(u_D^{k-1})$ by Lemma 4 and $\pi_D^{I(k)} \circ \pi_{I(k)}^D = \mathrm{Id}_{V_{I(k)}}$. Apply $\pi_{R(k)}^{I(k)}$ on both sides of (12) when $\Omega_{I(k-1)} \subset \Omega_{I(k)}$, then

$$
\pi_{R(k)}^{I(k)}(u_{R(k)}^{k,1}) = \pi_{R(k)}^{I(k)}(u_{R(k)}^{k,*}) + \pi_{R(k)}^{I(k)} \circ \pi_{I(k)}^{R(k)} \left(\pi_D^{I(k)}(u_D^{k-1}) - \pi_D^{I(k-1)}(u_D^{k-1}) \right).
\tag{19}
$$

Subtraction of (18) and (19) gives the second formula in (i).

(Part ii) Apply $\pi_D^{I(k)}$ on both sides of (13), then

$$
\pi_D^{I(k)}(u_D^{k,2}) = \pi_D^{I(k)} \circ (\mathrm{Id}_{V_D} - \pi_{I(k)}^D \circ \pi_D^{I(k)})(u_D^{k,1}) + \pi_D^{I(k)} \circ \pi_{I(k)}^D \circ \pi_{R(k)}^{I(k)}(u_{R(k)}^{k,2}) = \pi_{R(k)}^{I(k)}(u_{R(k)}^{k,2}).
$$

(Part iii) Apply $\pi_{R(k)}^{I(k)}$ on both sides of (15), then

$$
\pi_{R(k)}^{I(k)}(u_{R(k)}^{k,3}) = \pi_{R(k)}^{I(k)} \circ \pi_{I(k)}^{R(k)} \left(\pi_D^{I(k)}(u_D^{k,3}) \right) + \pi_{R(k)}^{I(k)} \left(u_{R(k)}^{k,2} - \pi_{I(k)}^{R(k)} \circ \pi_D^{I(k)}(u_D^{k,2}) \right).
$$

The formula (iii) can be obtained by replacing $\pi_D^{I(k)}(u_D^{k,2})$ in the above equation by $\pi_{R(k)}^{I(k)}(u_{R(k)}^{k,2})$ using formula (ii). $\quad\square$

Although $u_D^{k,1}$ (in the case of $\Omega_{I(k-1)} \subset \Omega_{I(k)}$) and $u_D^{k,3}$ are not identical to $u_{R(k)}^{k,1}$ and $u_{R(k)}^{k,3}$ when projected to $\Omega_{I(k)}$, respectively, we have the following conservation properties.

Theorem 5 (*Global Conservation*). *Assume $\int_{\Omega_{I(0)}} \pi_D^{I(0)} u_D^0 ds = \int_{\Omega_{R(0)}} u_{R(0)}^0 ds$, then for $k = 1, \ldots,$*

(a) $\int_{\Omega_{R(k)}} u_{R(k)}^{k,*} d\xi = \int_{\Omega_{R(k-1)}} u_{R(k-1)}^{k-1} d\xi$;

(b) $\int_{\Omega_D} u_D^{k,1} d\mathbf{x} = \int_{\Omega_D} u_D^{k-1} d\mathbf{x}$;

(c) $\int_{\Omega_{R(k)}} u_{R(k)}^{k,1} d\xi = \int_{\Omega_{R(k-1)}} u_{R(k-1)}^{k-1} d\xi$, *if $\Omega_{I(k-1)} \supseteq \Omega_{I(k)}$*;

(d) $\int_{\Omega_{R(k)}} u_{R(k)}^{k,1} d\xi = \int_{\Omega_{R(k-1)}} u_{R(k-1)}^{k-1} d\xi + \int_{\Omega_{I(k)}} \left(\pi_D^{I(k)} - \pi_D^{I(k-1)} \right)(u_D^{k-1}) ds$, *if $\Omega_{I(k-1)} \subset \Omega_{I(k)}$*;

(e) $\int_{\Omega_{I(k)}} \pi_D^{I(k)}(u_D^{k,1}) ds = \int_{\Omega_{R(k)}} u_{R(k)}^{k,1} d\xi$;

(f) $\int_{\Omega_{I(k)}} \pi_D^{I(k)}(u_D^{k,2}) ds = \int_{\Omega_{R(k)}} u_{R(k)}^{k,2} d\xi$;

(g) $\int_{\Omega_{I(k)}} \pi_D^{I(k)}(u_D^{k,3}) ds = \int_{\Omega_{R(k)}} u_{R(k)}^{k,3} d\xi$.

Proof. Equation (a) is a direct result of (10). With the help of the mass conservation properties of operators listed in Section 2.2, equations (c) and (d) are deduced from (12) and (a), the equation (e) from Theorem 4(i), and equations (f) and (g) from Theorem 4(ii) and (iii), respectively. As for (b), according to formula (11),

$$
\begin{aligned}
\int_{\Omega_D} u_D^{k,1} d\mathbf{x} &= \int_{\Omega_D} \left\{ u_D^{k-1} - \pi_{I(k-1)}^D \circ \pi_D^{I(k-1)}(u_D^{k-1}) + \pi_{I(k)}^D \circ \pi_{R(k)}^{I(k)}(u_{R(k)}^{k,*}) \right\} d\mathbf{x} \\
&\overset{\text{Lemma 2}}{=} \int_{\Omega_D} u_D^{k-1} d\mathbf{x} - h \int_{\Omega_{I(k-1)}} \pi_D^{I(k-1)}(u_D^{k-1}) d\mathbf{x} + h \int_{\Omega_{R(k)}} u_{R(k)}^{k,*} d\xi \\
&\overset{\text{(a)}}{=} \int_{\Omega_D} u_D^{k-1} d\mathbf{x} - h \int_{\Omega_{I(k-1)}} \pi_D^{I(k-1)}(u_D^{k-1}) d\mathbf{x} + h \int_{\Omega_{R(k-1)}} u_{R(k-1)}^{k-1} d\xi \\
&= \int_{\Omega_D} u_D^{k-1} d\mathbf{x},
\end{aligned}
$$

where in the last equality we have used an induction from the initial condition $\int_{\Omega_{I(0)}} \pi_D^{I(0)}(u_D^0) ds = \int_{\Omega_{R(0)}} u_{R(0)}^0 ds$. $\quad\square$
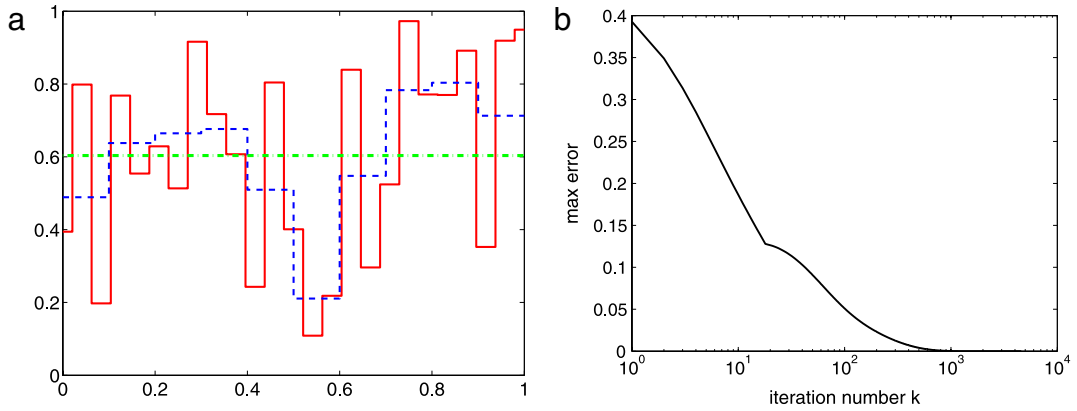
Fig. 3. (a) The initial data u_R (solid), its projection (dashline) to Ω_I, and the mean value $\bar{u}_R$ (dash–dot line). (b) The maximum error of $\|P^k(u) - \bar{u}_R\|_{\infty, \Omega_R}$ with respect to the iteration number k.
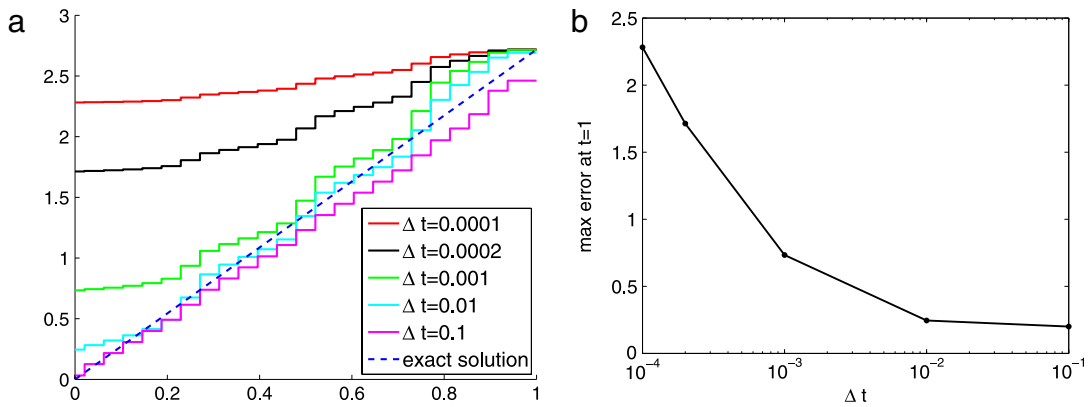
Fig. 4. (a) The numerical solutions and the exact solution at $t = 1$. The direct interpolation is used. (b) Maximum error with respect to time step size Δt.

3. Numerical simulations

3.1. Data smearing out by direct interpolation

If the capillaries remain stationary and the reaction rate f and the diffusion constant D are both zeros, then the exact solution u is equal to the initial data. However, if the direct data interpolation (16), instead of the proposed formula (14), is used, then the full numerical algorithm in Section 2.4 is just the iteration of the operator $P = \pi_R^R \circ \pi_R^I$. In the first example, we demonstrate how this process smears out the variation of data as proved in Theorem 2. The domain $\Omega_R = [0, 1]$ is divided into 25 intervals and the mesh points are $\xi_1^R = 0$, $\xi_i^R = \frac{2i-3}{2n}$, $(i = 2, \ldots, n+1)$, $\xi_{n+2}^R = 1$, where $n = 24$. The domain $\Omega_I = [0, 1]$ is divided into 10 equidistant intervals. In this way, the inner mesh points of Ω_R and Ω_I are disjoint. The initial data u_R is generated by a random generator and both u_R and its projection $\pi_R^I(u_R)$ are shown in Fig. 3(a). The maximum error, $\|P^k(u) - \bar{u}_R\|_{\infty, \Omega_R} = \max_{x \in \Omega_R} |P^k(u)(x) - \bar{u}_R|$, where $\bar{u}_R = \int_0^1 u_R(x)dx$ (the mean value of u_R over Ω_R), is plotted in Fig. 3(b), which shows the pointwise convergence of $P^k(u)$ to the mean value.

Next, we add a reaction on the capillary, $\frac{\partial u}{\partial t} = u$, $u(x, 0) = x$. All the others are the same as in the last example. The numerical solutions at $t = 1$ with different time step Δt values are shown in Fig. 4(a). Note that when Δt decreases, the numerical solutions become more uniform, which demonstrates the smearing property of the direct interpolation. The maximum error between the numerical solutions and the exact solution at $t = 1$ is shown in Fig. 4(b), where the error increases when Δt gets smaller. This surprising result is purely produced by the direct interpolation.

In contrast, if the proposed formula (14) is used, then the catastrophic effects in the above two examples will not occur and the true solution will be recovered.

3.2. Simulations of VEGF reaction and diffusion in angiogenesis

We use the Conservative and Variation Preserving Finite Volume Method in Section 2.4 to solve Eqs. (1) and (2). For the whole domain $\Omega = [0, 2 \text{ mm}]^2$, we choose the spatial mesh size $h = 0.02$ mm and the time step $\Delta t = 0.001$ days for
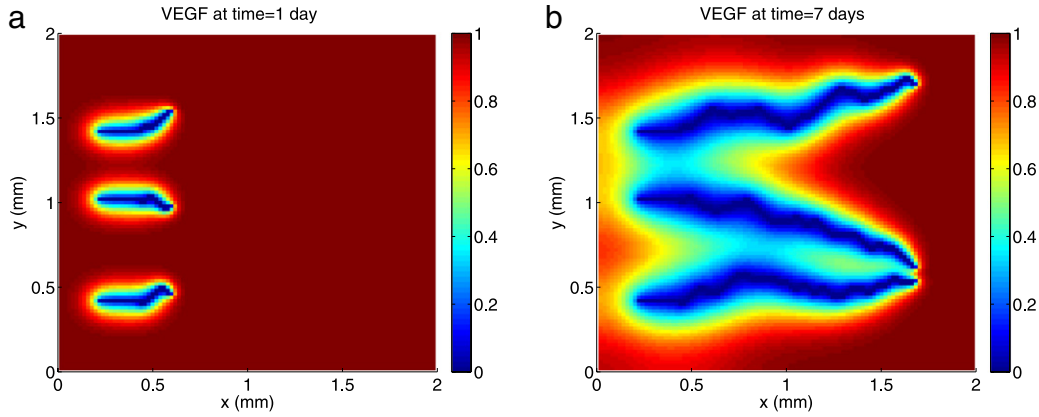
Fig. 5. Simulation results of VEGF concentration. The no-flux condition is applied on four edges of the domain. $D = 4 \times 10^3$ μm^2 day^{-1}. (a) $t = 1$ day, (b) $t = 7$ days.

all simulations in this subsection. The diffusion constant D ranges from 4×10^3 μm^2 day^{-1} to 4×10^6 μm^2 day^{-1}. Other parameters are: the VEGF reference value $C_0 = 3.33 \times 10^{-3}$ μM (equal to 1 in the color bar), total receptor concentration $R_T = 7.64 \times 10^{-3}$ μM. The parameters for VEGF/receptor kinetics are $k_{\text{on}} = 9.98 \times 10^4$ μM^{-1} day^{-1}, $k_{\text{off}} = 72.36$ day^{-1}, and $k_p = 16.08$ day^{-1}. The initial value of VEGF is set to be the reference value C_0 in the whole domain. All these parameters are also used in [15,3].

To model the capillary growth, we apply the algorithm in Section 2.1 In this work, we set $m = 501$, $s_m(0) = 0.2$ mm, $U = 0.36$ mm/day, $L_0 = 0.04$ mm, $p_1 = 0.8$, and $p_2 = 0.1$. The initial value of free receptor [FR] is R_T, and that of bound receptor [BR] is zero. Initially, these capillaries are of length 0.2 mm, therefore, the mesh size on the capillaries is 0.4 μm. When the capillary extends to the maximum length 2.72 mm at $t = 7$ days, the mesh size is 6 μm, still far less than the diffusion mesh size $h = 20$ μm. The capillaries at $t = 7$ days are shown in Fig. 9(a) and (b).

In the first group of simulations, we enforce the no-flux condition on all the four edges of the square domain and investigate the growth factor uptake by capillaries with three different diffusion constants: $D = 4 \times 10^3, 4 \times 10^4, 4 \times 10^5$ μm^2 day^{-1}. The results at day $t = 1$ and $t = 7$ are shown in Figs. 5–7. With the no-flux boundary condition, the growth factor will drop to zero level due to capillary uptake given sufficient time. When the capillaries are extending, the endothelial cells are consuming VEGF, therefore the VEGF concentration keeps decreasing along the paths of capillaries. When D is the smallest, most growth factor in the domain remains at day 7, and the capillary path is clearly seen in this case (Fig. 5). When D increases to 4×10^4 μm^2 day^{-1}, more growth factor molecules are consumed by capillaries (Fig. 6(b)), and when D increases to 4×10^5 μm^2 day^{-1} the growth factor has vanished at 7 days (Fig. 7(b)). It is interesting to observe that the growth factor concentration is higher in the front of the capillaries than the rear, which can be clearly seen from Fig. 6(b). This is because the capillary is extending into the high concentration region. The free and bound receptor densities on one of three capillaries are shown in Fig. 8 for $D = 4 \times 10^3, 4 \times 10^4$ μm^2 day^{-1}. The oscillation of data is due to the change of directions of capillaries. The bound receptor density is higher near the tip because the tip always migrates into a new location with higher growth factor value. The receptors quantities near the capillary tip are of smaller gradient magnitude for larger diffusion constant.

Next, we study the growth factor uptake when the boundary condition of growth factor on the right edge $x = 2$ mm is changed to $u = 3.33 \times 10^{-3}$ μM, that is, the right edge serves as the source of VEGF. The results for $4 \times 10^5, 4 \times 10^6$ μm^2 day^{-1} are shown in Fig. 9. In contrast to the results in the first group, when the diffusion constant is larger, the growth factor concentration in the whole domain is higher, because the source of growth factor continuously provides new growth factor into the domain and the larger diffusion indicates more compensation for the capillary uptake (Fig. 9(a), (b)). With increased growth factor concentration for larger diffusion constant, the bound receptor density is also larger and distribution along the capillary is less oscillatory (Fig. 9(c), (d)).

4. Conclusions

In this paper, we developed a conservative and variation preserving finite volume method when the reaction mesh and the diffusion mesh are not overlapping. The numerical method not only reserves the mass during data transfer but also retains the spatial variation along the capillary. Numerical examples show that the direct interpolation has the risk of creating purely artificial effects and smearing out the data.

Our novel data transfer algorithm is similar to the wavelet method which is used in a multiscale reaction–diffusion model [16]. However, the wavelet method in [16] is only applicable to a fixed straight-line reaction domain and uniform reaction meshes. In contrast, our algorithm can handle the non-uniform spatial discretization and arbitrary shaped reaction domains whose shape and length are constantly changing in time.
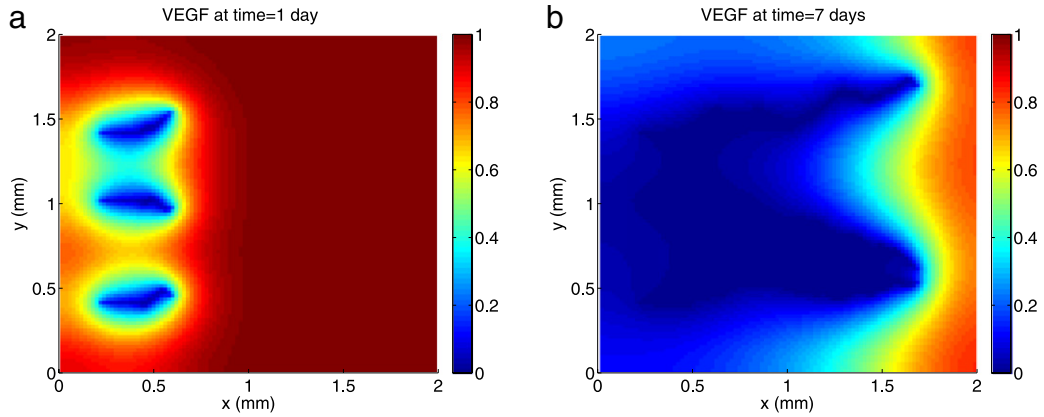
Fig. 6. Simulation results of VEGF concentration. The no-flux condition is applied on four edges of the domain. $D = 4 \times 10^4 \ \mu m^2 \ day^{-1}$. (a) $t = 1$ day, (b) $t = 7$ days.
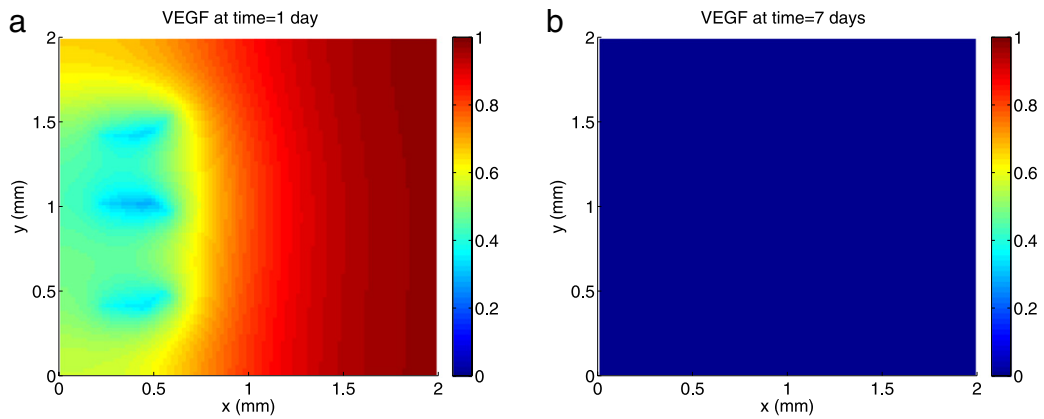

Fig. 7. Simulation results of VEGF concentration. The no-flux condition is applied on four edges of the domain. $D = 4 \times 10^5 \ \mu m^2 \ day^{-1}$. (a) $t = 1$ day, (b) $t = 7$ days.
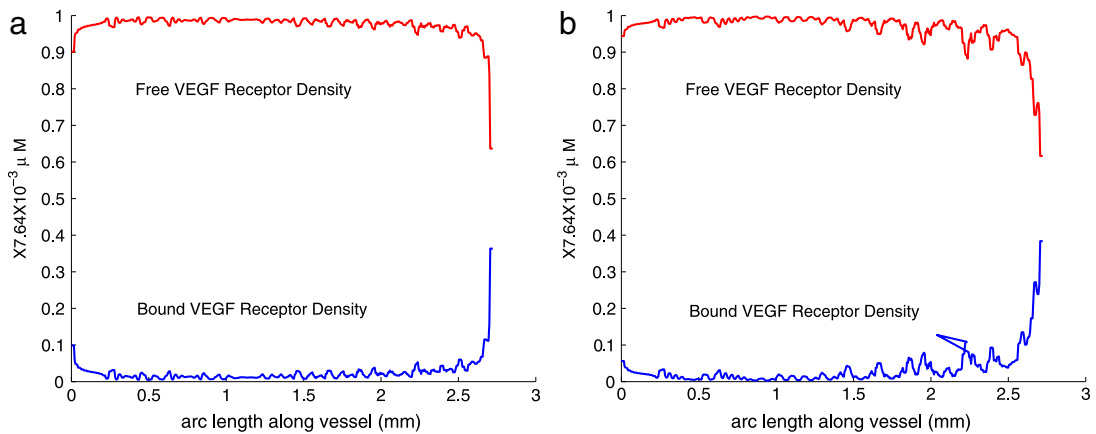
Fig. 8. Simulation results on one capillary at $t = 7$ days. The no-flux condition is applied on four edges of the domain. (a) $D = 4 \times 10^3 \ \mu m^2 \ day^{-1}$. (b) $D = 4 \times 10^4 \ \mu m^2 \ day^{-1}$.

In this work, the reactions are modeled by ordinary differential equations. Nevertheless, the reactions can also be modeled by other methods such as stochastic equations as in [17,16], which can be easily incorporated in our algorithm. In this work the capillaries grow along the diffusion domain meshlines. But our algorithm can be applied with slight modifications to any non-lattice capillary growth model which produces more realistic vasculature morphology such as the stochastic model of [7], the circular random walk model of [5], and the cell-based model of [3]. Although this study is for the 2-D case, the
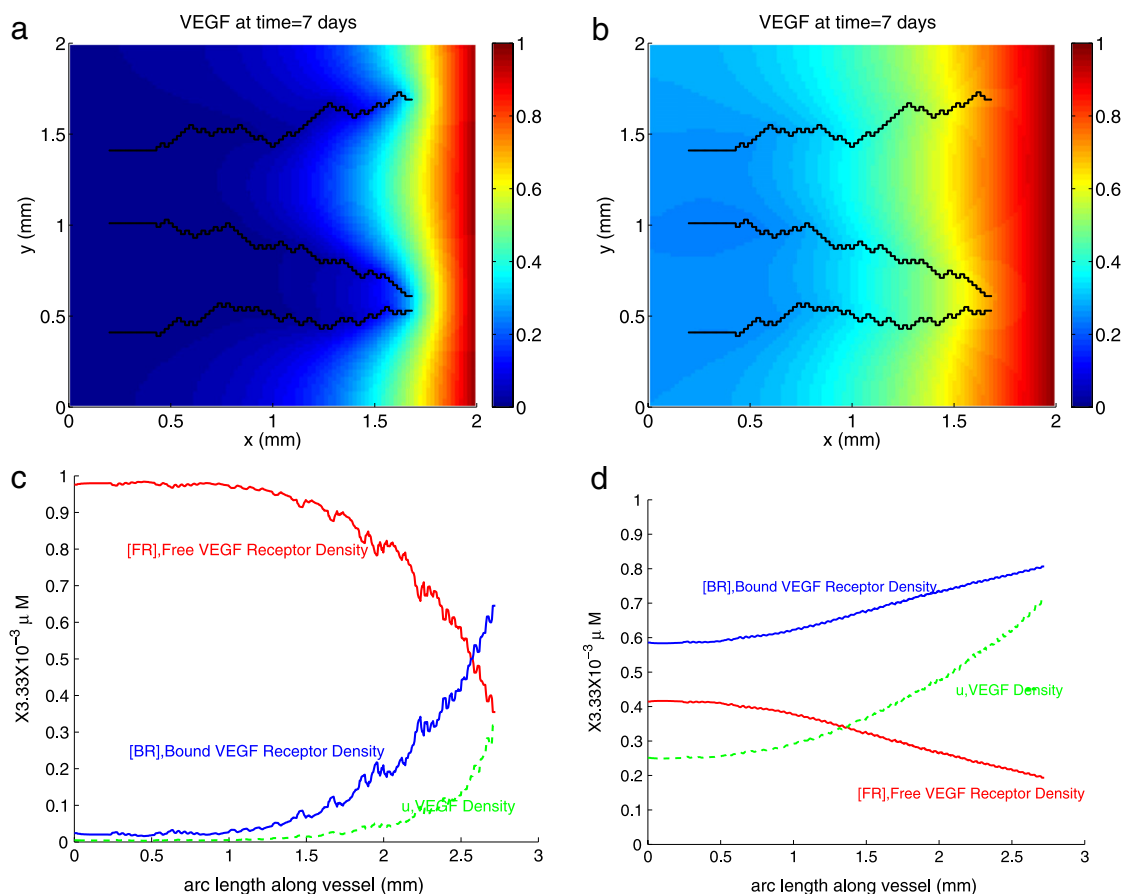
Fig. 9. Simulation results at $t = 7$ days. The boundary condition is $u = 3.33 \times 10^{-3}$ μM at $x = 2$ mm and no-flux condition on other three edges. (a, c) $D = 4 \times 10^5$ μm^2 day^{-1}. (b, d) $D = 4 \times 10^6$ μm^2 day^{-1}.

numerical method can be straightforwardly extended to the 3-D case (see Remark 2) and all the properties still hold except that Lemma 2 requires a slight modification (see Remark 1).

Acknowledgment

Appendix A. Supplementary data

Supplementary material related to this article can be found online at http://dx.doi.org/10.1016/j.cam.2014.08.002.

References

[1] M.M. Sholley, G.P. Ferguson, H.R. Seibel, J.L. Montour, J.D. Wilson, Mechanisms of neovascularization. Vascular sprouting can occur without proliferation of endothelial cells, Lab. Invest. 51 (1984) 624–634.
[2] D. Hanahan, J. Folkman, Patterns and emerging mechanisms of the angiogenic switch during tumorigenesis, Cell 86 (1996) 353–364.
[3] T. Jackson, X. Zheng, A cell-based model of endothelial cell migration, proliferation and maturation during corneal angiogenesis, Bull. Math. Biol. 72 (2010) 830–868.
[4] X. Zheng, G.Y. Koh, T. Jackson, A continuous model of angiogenesis: initiation, extension, and maturation of new blood vessels modulated by vascular endothelial growth factor, angiopoietins, platelet-derived growth factor-*B*, and pericytes, Discrete Contin. Dyn. Syst. Ser. B 18 (4) (2013) 1109–1154.
[5] M.J. Plank, B.D. Sleeman, Lattice and non-lattice models of tumour angiogenesis, Bull. Math. Biol. 66 (2004) 1785–1819.
[6] A.R.A. Anderson, M.A.J. Chaplain, Continuous and discrete mathematical models of tumor-induced angiogenesis, Bull. Math. Biol. 60 (1998) 857–900.
[7] C.L. Stokes, D.A. Lauffenburger, Analysis of the roles of microvessel endothelial cell random mobility and chemotaxis in angiogenesis, J. Theoret. Biol. 152 (1991) 377–403.
[8] S. Tong, F. Yuan, Numerical simulations of angiogenesis in the cornea, Microvasc. Res. 61 (2001) 14–27.
[9] S. Sun, M.F. Wheeler, M. Obeyesekere, C. Patrick, A deterministic model of growth factor-induced angiogenesis, Bull. Math. Biol. 67 (2005) 313–337.
[10] V. Capasso, D. Morale, Stochastic modelling of tumour-induced angiogenesis, J. Math. Biol. 58 (2009) 219–233.
[11] N. Mantzaris, S. Webb, H.G. Othmer, Mathematical modeling of tumor-induced angiogenesis, J. Math. Biol. 49 (2004) 111–187.

[12] B.J. Vakoc, R.M. Lanning, J.A. Tyrrell, T.P. Padera, L.A. Bartlett, T. Stylianopoulos, L.L. Munn, G.J. Tearney, D. Fukumura, R.K. Jain, B.E. Bouma, Three-dimensional microscopy of the tumor microenvironment *in vivo* using optical frequency domain imaging, Nat. Med. 15 (2009) 1219–1223.
[13] J. Stoer, R. Bulirsch, Introduction to Numerical Analysis, third ed., Springer, 2010.
[14] R. Eymard, T. Gallouët, R. Herbin, Finite volume methods, Handb. Numer. Anal. 7 (2000) 713–1018.
[15] F. Mac Gabhann, A.S. Popel, Model of competitive binding of vascular endothelial growth factor and placental growth factor to VEGF receptors on endothelial cells, Am. J. Physiol. Heart Circ. Physiol. 286 (1) (2004) H153–H164.
[16] S.K. Mishra, K. Muralidharan, P. Deymier, G. Frantziskonis, S. Simunovic, S. Pannala, Wavelet-based spatial scaling of coupled reaction–diffusion fields, Int. J. Multiscale Comput. Eng. 6 (2008) 281–297.
[17] T. Alarcon, K.M. Page, Stochastic models of receptor oligomerization by bivalent ligand, J. R. Soc. Interface 3 (2006) 545–559.